FULL PAPER

Dalton
www.rsc.org/dalton

Macrocyclic ligand design. Interaction of a series of successively N-benzylated derivatives of 1,4,8,11-tetraazacyclotetradecane (cyclam) with copper(II) and nickel(II)

Ying Dong,[a] Geoffrey A. Lawrance,[b] Leonard F. Lindoy*[a] and Peter Turner[a]

[a] *Centre for Heavy Metals Research, School of Chemistry, The University of Sydney, N.S.W. 2006, Australia*

[b] *Discipline of Chemistry, School of Environmental and Life Sciences, The University of Newcastle, Callaghan 2308, Australia*

Received 20th November 2002, Accepted 17th February 2003
First published as an Advance Article on the web 18th March 2003

The interaction of a series of N-benzylated cyclam ligand derivatives incorporating from one to four benzyl groups with nickel(II) and copper(II) is reported. The isolation of a selection of 1 : 1 (metal : ligand) complexes of both metals has been carried out and visible spectral, EPR, electrochemical and X-ray determinations have been employed to probe the nature of the respective complexes in both the solid state and in solution. Emphasis has been given to investigating the effect of the successive N-benzylation along this ligand series on the properties of the above complexes. The UV–VIS spectra obtained for each series of metal complexes indicate that the sequential introduction of N-benzyl substituents produces a change to lower ligand fields of the corresponding macrocyclic tetramines. Cyclic voltammograms of both the nickel(II) (low-spin) and copper(II) complexes both yield evidence for M(III)/M(II) as well as M(II)/M(I) couples in acetonitrile.

Introduction

The modification of tetra-aza macrocyclic ligands to control and tune the redox properties of coordinated metal centres has been the subject of continuing interest.[1] Variations can be introduced by altering the size of the macrocyclic ring or by placing substituents on the nitrogen donors and/or the ring framework. Of these approaches, N-substitution of the donor atoms has the potential to generate the biggest steric and electronic effects, due to the closeness of the site of substitution to introduced metal ions. For example, since they raise the steric bulk of the molecule their presence may tend to inhibit the coordination of additional donors in the coordination sphere. Thus, apart from an anticipated effect on the redox properties of metal complexes, structural and spectroscopic effects arising from N-substitution are anticipated.

Previous work by us has been concerned with the synthesis of a series of N-benzylated cyclam ligand derivatives incorporating from one to four benzyl groups.[2] These represent excellent candidates for a comparative study of the effects of such substitution on the metal binding properties towards selected metal ions. In the present study we report the results of an investigation of the interaction of **1**–**5** with nickel(II) and copper(II), with emphasis on the effect of the successive benzylation on the structural, spectral and electrochemical properties of these complexes. The results are also compared with the behaviour of the unsubstituted parent macrocycle **6** (cyclam).

Experimental

Where available, all commercial reagents and solvents were of analytical or HPLC grade. The preparation of ligands **1**–**5** has been reported previously[2] 1,4,8,11-Tetraazacyclotetradecane (cyclam; **6**) was prepared by the published procedure.[3]

Solid state UV–VIS spectra were measured on a CARY 1E UV–VISible spectrophotometer (samples spread on filter paper) while solution UV–VIS spectra (at $(5 \pm 4) \times 10^{-3}$ mol dm^{-3}) were obtained on a CARY 5E UV–VIS-NIR spectrophotometer on solutions. EPR spectra were obtained on samples as dimethylformamide glasses at 77 K using a Bruker EMX EPR spectrometer at 9.464 GHz (X-band). Atomic absorption spectroscopy data were obtained on a SpectrAA·800 spectrometer. X-Ray diffraction data were obtained on a Bruker SMART 1000 CCD diffractometer.

Table 1 Conductance values for nickel(II) and copper(II) complexes of **1**–**6**

Complex	Colour	Λ^a/S cm² mol^{-1}
[Ni(**1**)]$(ClO_4)_2$	Orange	126
[Ni(**2**)]$(ClO_4)_2$	Orange	125
[Ni(**3**)]$(ClO_4)_2$	Orange	–
[Ni(**4**)]$(ClO_4)_2$	Orange	122
[Ni(**6**)]$(ClO_4)_2$	Orange	126
[Cu(**1**)$(NO_3)_2$]·0.5MeOH	Purple	89
[Cu(**2**)$(NO_3)_2$]·MeOH	Blue	73
[Cu(**3**)(NO_3)]NO_3	Blue	85
[Cu(**4**)(NO_3)]NO_3	Blue	86
[Cu(**5**)(H_2O)]$(NO_3)_2$·EtOH·H_2O	Green	106
[Cu(**6**)(NO_3)]NO_3	Purple	96

[a] Conductance at 25 °C in methanol at ~10^{-3} mol dm^{-3}; expected range for a 1 : 1 electrolyte in methanol is 80–115 S cm² mol^{-1} while that for a 2 : 1 electrolyte is 160–220 S cm² mol^{-1}.

Cyclic voltammetry studies were performed using a conventional three-electrode configuration with *iR* compensation and a BAS Model 100B electrochemical system, controlled by a computer using the BAS software. The working electrodes employed were glassy carbon or platinum discs. The reference electrode was Ag/AgCl and was separated from the working and Pt wire auxiliary electrodes by a glass sleeve fitted with a Vycor frit. Solutions were prepared in HPLC-grade acetonitrile or acetone, 0.1 mol dm^{-3} in *n*-$Bu_4N(ClO_4)$, and were purged with argon gas. Complex concentrations in the millimolar range were used throughout. For the ferrocenium/ferrocene reference couple, $E_{1/2}$ was at +0.52 V (acetonitrile) and +0.50 V (acetone) under these conditions. Scans were measured over the range 10–5000 mV s^{-1}, with reported results being mainly those recorded at 100 mV s^{-1}. Aspects of the electrochemical results are illustrated in Figs. 1–5.

Physical, spectral and electrochemical data for the complexes are summarised in Tables 1–4.

DOI: 10.1039/b211394e

Table 2 UV–VIS spectrophotometric data for the nickel(II) and copper(II) complexes of cyclam and **1**–**5**

Complex	λ_{max} [a]/nm	λ_{max} [b]/nm (ε/M^{-1} cm^{-1})	λ_{max} [c]/nm (ε/M^{-1} cm^{-1})
[Cu(**6**)](NO$_3$)$_2$	508	505 (88)	511 (58)
[Cu(**1**)](NO$_3$)$_2$	524	510 (112)	520 (90)
[Cu(**2**)](NO$_3$)$_2$	539	525 (129)	545 (126)
[Cu(**3**)](NO$_3$)$_2$	543	544 (301)	550 (240)
[Cu(**4**)](NO$_3$)$_2$	560	562 (235)	583 (223)
[Cu(**5**)](NO$_3$)$_2$	629	545 (420)	699 (285)
[Ni(**6**)](ClO$_4$)$_2$	459		322 (sh), 461 (13), 651 (vw), 935 (vw)
[Ni(**1**)](ClO$_4$)$_2$	473		332 (sh), 480 (15), 704 (vw), 995 (vw)
[Ni(**2**)](ClO$_4$)$_2$	478		341 (sh), 515 (10), 751 (vw), 974 (vw)
[Ni(**3**)](ClO$_4$)$_2$	471		334 (sh), 476 (24), 798 (vw), 1016 (vw)
[Ni(**4**)](ClO$_4$)$_2$	488		348 (sh), 517 (10), 820 (vw), 1030 (vw)

[a] Solid state UV–VIS spectra. [b] Spectra were recorded in methanol. Spectra for the nickel(II) complexes in this solvent were not obtained due to their poor solubility. [c] Spectra were obtained in acetonitrile.

Table 3 EPR spectroscopic parameters for the copper(II) complexes of **1**–**6**

Complex	$g_{\|\|}$	$g_{\perp}$	$A_{\|\|}$/G
[Cu(**1**)](NO$_3$)$_2$	2.178	2.044	196
[Cu(**2**)](NO$_3$)$_2$	2.179	2.055	194
[Cu(**3**)](NO$_3$)$_2$	2.182	2.050	182
[Cu(**4**)](NO$_3$)$_2$	2.198	2.049	176
[Cu(**5**)](NO$_3$)$_2$	2.225	2.035	155
[Cu(**6**)](NO$_3$)$_2$	2.173	2.048	200

X-Ray structure determinations

Full sphere data were collected at 150(2) K, with the exception of the Cu(**1**) and Cu(**3**) complexes for which data were collected at 294(2) K. Data were collected with ω scans to 56° 2θ using a Bruker SMART 1000 CCD diffractometer employing graphite monochromated Mo-Kα radiation generated from a sealed tube (0.71073 Å). A recollection of the reflections in the first 50 CCD frames at the end of the collection showed no significant change in intensities. In general a Gaussian absorption correction was applied to the data with XPREP,[4,5] as was a further empirical correction determined with SADABS.[6] An additonal empircial correction was not used for the Ni(3) complex data. The data integration and reduction were undertaken with SAINT and XPREP,[4] and subsequent computations were carried out with the teXsan,[6] WinGX[7] and XTAL[8] graphical user interfaces. The structures were solved by direct methods using SIR97,[9] and extended and refined with SHELXL-97.[10] In general, the non-hydrogen atoms were modelled with anisotropic thermal parameters and a riding atom model was used for the hydrogen atom. The non-hydrogen methanol sites were modelled with isotropic displacement parameters. ORTEP[11] depictions of the molecules with 20% displacement ellipsoids are provided provided in Figs. 6–10, and pertinent geometry details are listed in Tables 5–8.

Table 5 Bond lengths (Å) and angles (°) for [Cu(**1**)(NO$_3$)$_2$]·0.5MeOH and [Cu(**2**)(NO$_3$)$_2$]·MeOH

	Cu(**1**)(NO$_3$)$_2$	Cu(**2**)(NO$_3$)$_2$
Cu(1)–O(1)	2.804(6)	2.7325(15)
Cu(1)–O(4)	2.476(4)	2.5663(13)
Cu(1)–N(1)	2.061(4)	2.0708(12)
Cu(1)–N(2)	1.997(5)	2.0719(12)
Cu(1)–N(3)	2.027(5)	2.0207(13)
Cu(1)–N(4)	2.010(5)	2.0272(13)
N(1)–Cu(1)–N(2)	93.77(18)	96.51(5)
N(1)–Cu(1)–N(3)	177.93(17)	175.66(5)
N(1)–Cu(1)–N(4)	86.40(18)	86.55(5)
N(2)–Cu(1)–N(3)	86.2(2)	86.18(5)
N(2)–Cu(1)–N(4)	179.07(19)	175.21(5)
N(3)–Cu(1)–N(4)	93.6(2)	90.55(5)
N(1)–Cu(1)–O(1)	98.05(16)	98.37(4)
N(1)–Cu(1)–O(4)	91.70(16)	91.15(4)
N(2)–Cu(1)–O(1)	92.1(2)	92.67(4)
N(2)–Cu(1)–O(4)	87.74(18)	87.18(4)
N(3)–Cu(1)–O(1)	79.88(18)	84.86(5)
N(3)–Cu(1)–O(4)	90.37(18)	85.57(5)
N(4)–Cu(1)–O(1)	88.8(2)	90.52(4)
N(4)–Cu(1)–O(4)	91.34(19)	89.08(4)
O(1)–Cu(1)–O(4)	170.24(16)	170.42(4)

Crystal and structure refinement data

The refinement residuals are defined as

$R1 = \Sigma||F_o| - |F_o||/\Sigma|F_o|$ for $F_o > 2\sigma(F_o)$ and $wR2 = (\Sigma w(F_o^2 - F_c^2)^2/\Sigma(wF_c^2)^2)^{1/2}$ all reflections where $w = 1/[\sigma^2(F_o^2) + (AP)^2 + BP]$, $P = (F_o^2 + 2F_o^2)/3]$ and A and B are as listed below.

[CuL(NO$_3$)$_2$]·0.5MeOH (L = **1**): $C_{17.5}H_{32}CuN_6O_{6.5}$, M = 494.03, monoclinic, space group $C2/c$ (#15), a = 16.0210(17), b = 19.181(2), c = 15.6723(16) Å, β = 104.095(2)°, V = 4671.1(8) Å^3, D_c (Z = 8) = 1.405 g cm^{-3}, crystal size 0.370 × 0.247 × 0.094 mm, colour red, habit prism, μ(Mo-Kα) = 0.981

Table 4 Observed M(II)/(I) and M(III)/(II) couples from cyclic voltammograms of copper(II) and nickel(II) complexes of ligands shown [glassy carbon working electrode, 100 mV s^{-1} scan rate, acetonitrile/0.1 M Bu$_4$N(ClO$_4$), 1 mM complex, $E_{1/2}$ (or E_p for irreversible couples) *vs.* Ag/AgCl]

Complex	M(III)/(II), $E_{1/2}$/V (ΔE/mV)	M(II)/(I), $E_{1/2}$/V (ΔE/mV)
[Cu(**6**)](NO$_3$)$_2$	+1.377 (irrev.)	−0.853 (85)
[Cu(**1**)](NO$_3$)$_2$	+1.442 (irrev.)	−0.640 (110)
[Cu(**2**)](NO$_3$)$_2$	+1.495 (irrev.)	−0.430 (230)
[Cu(**3**)](NO$_3$)$_2$	+1.540 (irrev.)	−0.406 (120)
[Cu(**4**)](NO$_3$)$_2$	+1.570 (irrev.)	−0.175 (75)
[Cu(**5**)](NO$_3$)$_2$	+1.630 (irrev.)	+0.042 (105)
[Ni(**6**)](ClO$_4$)$_2$	+1.100 (75), +0.583 (70)	−1.447 (225)
[Ni(**1**)](ClO$_4$)$_2$	+1.074 (205), +0.734 (100)	−1.310 (110)
[Ni(**2**)](ClO$_4$)$_2$	+1.248 (215), +0.925 (70)	−1.217 (200)
[Ni(**3**)](ClO$_4$)$_2$	+1.402 (80), +1.015[a]	−1.011 (60)
[Ni(**4**)](ClO$_4$)$_2$	+1.52[a], +1.19[a]	−0.917 (105)

[a] Reversibility limited or masked by adsorption phenomena.

Table 6 Bond lengths (Å) and angles (°) for [Ni(**3**)](ClO$_4$)$_2$

Ni(1)–N(1)	1.9701(15)
Ni(1)–N(2)	1.9441(16)
N(1)–Ni(1)–N(2)	92.95(7)

Table 7 Bond lengths (Å) and angles (°) for [Cu(**3**)(NO$_3$)]NO$_3$

Cu(1)–O(1)	2.6571(8)
Cu(1)–N(1)	2.1085(15)
Cu(1)–N(2)	1.9898(13)
N(1)–Cu(1)–O(1)	94.56(4)
N(1)–Cu(1)–N(2)^a	86.20(5)
N(1)–Cu(1)–N(2)	93.80(5)
N(2)–Cu(1)–O(1)	86.94(4)

^{a} 1 − x, −y, 1 − z.

Table 8 Bond lengths (Å) and angles (°) [Cu(**5**)(H$_2$O)](NO$_3$)$_2$·2MeOH

Cu(1)–O(1)	2.226(2)
Cu(1)–N(1)	2.145(2)
Cu(1)–N(2)	2.0841(18)
N(1)–Cu(1)–N(1)^a	177.08(8)
N(2)–Cu(1)–N(2)^a	150.76(9)
N(1)–Cu(1)–N(2)	85.67(6)
N(1)–Cu(1)–N(2)^a	93.59(7)
N(1)–Cu(1)–O(1)	104.62(5)
N(2)–Cu(1)–O(1)	91.46(4)

^{a} 1 − x, y, 1/2 − z.

mm^{-1}, T(Gausian)$_{min,max}$ = 0.732, 0.914, 2θ_{max} = 56.58, *hkl* range −20 to 20, −25 to 24, −20 to 20, N = 24546, N_{ind} = 5563 (R_{merge} = 0.0412), N_{obs} = 2672 ($I > 2\sigma(I)$), N_{var} = 280, residuals $R1(F)$ = 0.0672, $wR2(F^2)$ = 0.2226, A = 0.07, B = 10.0, GoF(all) = 1.235, $\Delta\rho_{min,max}$ = −0.596, 0.707 e$^-$ Å^{-3}.

Individual features. The asymmetric unit contains a complex molecule with weakly coordinated nitrate counter ions and a methanol solvate molecule. The occupancy of the methanol sites was refined and then fixed at 0.5. The large N(5) nitrate ellipsoids evident in Fig. 6 may be the result of disorder arising from the partial occupancy of the methanol molecule, with which it interacts.

[CuL(NO$_3$)$_2$]·MeOH (L = **2**): $C_{25}H_{40}CuN_6O_7$, M = 600.17, monoclinic, space group $P2_1/c$ (#14), a = 13.316(3), b = 18.311(4), c = 12.303(3) Å, β = 113.132(4)°, V = 2758.6(11) Å^3, D_c (Z = 4) = 1.445 g cm^{-3}, crystal size 0.331 × 0.287 × 0.177 mm, colour purple, habit prism, μ(Mo-Kα) 0.846 mm^{-1}, T(Gausian)$_{min,max}$ = 0.744, 0.878, 2θ_{max} = 56.50, *hkl* range −17 to 16, −24 to 24, −16 to 16, N = 28625, N_{ind} = 6560 (R_{merge} = 0.0263), N_{obs} = 5778 ($I > 2\sigma(I)$), N_{var} = 354, residuals $R1(F)$ = 0.0304, $wR2(F^2)$ = 0.0869, A = 0.052, B = 1.08, GoF(all) = 1.031, $\Delta\rho_{min,max}$ = −0.566, 1.077 e$^-$ Å^{-3}.

Individual features. The asymmetric unit contains the complex molecule, two nitrate counter ions and a methanol solvate molecule.

[CuL(NO$_3$)$_2$] (L = **3**): $C_{24}H_{36}CuN_6O_6$, M = 568.13, monoclinic, space group $P2_1/c$ (#14), a = 9.9521(19), b = 11.851(2), c = 10.868(2) Å, β = 97.436(3)°, V = 1271.1(4) Å^3, D_c (Z = 2) = 1.484 g cm^{-3}, crystal size 0.265 × 0.173 × 0.088 mm, colour purple, habit tabular, μ(Mo-Kα) = 0.911 mm^{-1} T(Gausian)$_{min,max}$ = 0.794, 0.924, 2θ_{max} = 56.64, *hkl* range −12 to 13, −15 to 15, −14 to 14, N = 11469, N_{ind} = 3008 (R_{merge} = 0.0249), N_{obs} = 2523 ($I > 2\sigma(I)$), N_{var} = 169, residuals $R1(F)$ = 0.0292, $wR2(F^2)$ = 0.0835, A = 0.0481, B = 0.473, GoF(all) = 0.985, $\Delta\rho_{mim,max}$ = −0.193, 0.317 e$^-$ Å^{-3}.

Individual features. The asymmetric unit conatins half a complex located on an inversion centre.

[CuL(H$_2$O)](NO$_3$)$_2$·2MeOH (L = **5**): $C_{40}H_{58}CuN_6O_9$, M = 830.46, monoclinic, space group $C2/c$ (#15), a = 24.200(12), b = 9.471(5), c = 18.229(9) Å, β = 100.129(9)°, V = 4113(4) Å^3, D_c = 1.341 (Z = 4) g cm^{-3}, crystal size 0.216 × 0.183 × 0.117 mm, colour blue, habit prismatc, μ(Mo-Kα) = 0.592 mm^{-1}, T(Gausian)$_{min,max}$ = 0.863, 0.936, 2θ_{max} = 56.58, *hkl* range −30 to 30, −12 to 12, −23 to 24, N = 21311, N_{ind} = 4881 (R_{merge} = 0.0351), N_{obs} = 4183 ($I > 2\sigma(I)$), N_{var} = 260, residuals $R1(F)$ = 0.0479, $wR2(F^2)$ = 0.1420, A = 0.0936, B = 3.68, GoF(all) = 1.072, $\Delta\rho_{min,max}$ = −0.646, 0.872 e$^-$ Å^{-3}.

Individual features. The asymmetric unit contains half of the complex molecule centred on a two-fold axis passing through Cu(1) and O(1). The asymmetric unit also contains a methanol solvate molecule and a nitrate counter ion. The water hydrogen was located and modelled with an isotropic displacement parameter and a distance restraint.

[NiL](ClO$_4$)$_2$ (L = **3**): $C_{24}H_{36}Cl_2N_4NiO_8$, M = 638.18, monoclinic, space group $P2_1/c$ (#14), a = 9.0053(10), b = 17.8845(19), c = 8.6964(9) Å, β = 104.909(2)°, V = 1353.5(3) Å^3, D_c = 1.566 g cm^{-3}, Z = 2, crystal size 0.352 × 0.337 × 0.206 mm, colour orange, habit primatic, temperature = 294(2) K, μ(Mo-Kα) = 0.970 mm^{-1}, T(Gausian)$_{mim,max}$ = 0.698, 0.834, 2θ_{max} = 56.54, *hkl* range −11 to 11, −23 to 23, −11 to 11, N = 13290, N_{ind} = 3219 (R_{merge} = 0.0241), N_{obs} = 2876 ($I > 2\sigma(I)$), N_{var} = 178, residuals $R1(F)$ = 0.0349, $wR2(F^2)$ = 0.1008, A = 0.05, B = 0.5, GoF(all) = 1.202, $\Delta\rho_{mim,max}$ = −0.387, 0.670 e$^-$ Å^{-3}.

Individual features. The asymmetric unit contains the half of the complex molecule residing on an inversion centre, and a perchlorate counter ion.

CCDC reference numbers 198031–198035.

See http://www.rsc.org/suppdata/dt/b2/b211394e/ for crystallographic data in CIF or other electronic format.

Copper(II) solvent extraction

The solvent extraction experiments were carried out in screw top glass vials containing a chloroform phase (5 cm^3) and an aqueous phase (5 cm^3). The aqueous phase consisted of an unbuffered copper(II) nitrate solution (1 × 10^{-3} mol dm^{-3}) and was maintained at a pH of 5.00 ± 0.05 or 5.80 ± 0.05 by careful addition using a microsyringe of dilute sodium hydroxide or nitric acid during the course of the respective extraction experiments. The chloroform phase (which had been presaturated with distilled water) contained a ligand chosen from **1**–**5** at a concentration of 1 × 10^{-3} mol dm^{-3}, with a four-fold amount of palmitic acid also present. Control experiments contained only the corresponding concentration of palmitic acid in the organic phase and under the conditions employed no extraction of copper(II) was observed in this case. All experiments involved shaking the extraction vial for 24 h at 25 °C. The fraction of metal extracted was calculated as: [moles of metal ion in the organic phase]/[total number of moles of the metal in both phases]. The experiments were performed in duplicate with the relative error being approximately ±10%.

Metal complex synthesis

All complexes were dried over P_4O_{10} in a vacuum before microanalysis.

[Cu(1)(NO$_3$)$_2$]·0.5MeOH. Copper(II) nitrate–hydrate (2/5) (0.24 g, 1 mmol) in methanol (5 cm^3) was added to a solution of **1** (0.29 g, 1 mmol) in methanol (15 cm^3). The solution was stirred and heated for 0.5 h and the solvent was removed under reduced pressure. The residue was recrystallized from a mixture of dichloromethane and methanol to yield red–purple crystals (0.30 g, 60%). Single crystals suitable for X-ray diffraction were obtained from dichloromethane–methanol (1 : 1) (Found: C, 42.68; H, 6.70; N, 16.89. $C_{17.5}H_{32}CuN_6O_{6.5}$ requires C, 42.55; H, 6.53; N, 17.01%).

[Ni(1)](ClO$_4$)$_2$. Nickel(II) perchlorate hexahydrate (0.18 g, 0.5 mmol) in methanol (5 cm^3) was added to a solution of **1** (0.15 g, 0.5 mmol) in methanol (15 cm^3). The solution was stirred and heated for 0.5 h and the orange solution was left to stand at room temperature overnight. The golden yellow crystals that formed were filtered off and recrystallized from methanol (0.15 g, 65%) (Found: C, 37.31; H, 5.63; N, 10.03. $C_{17}H_{30}Cl_2NiN_4O_8$ requires C, 37.26; H, 5.53; N, 10.22%).

[Cu(2)(NO$_3$)$_2$]·MeOH. A similar procedure to that described for [Cu(**1**)(NO$_3$)$_2$]·0.5MeOH was employed. The crude product was recrystallized from methanol to yield blue crystals (yield 62%). Single crystals suitable for X-ray diffraction were obtained from dichloromethane–methanol (Found: C, 49.88; H, 6.59; N, 14.08. $C_{25}H_{40}CuN_6O_7$ requires C, 50.03, H, 6.72; N, 14.00%).

[Ni(2)](ClO$_4$)$_2$. A similar procedure to that described for [Ni(**1**)](ClO$_4$)$_2$ was employed. The crude product was purified by recrystallization from methanol to give orange crystals (yield 50%) (Found: C, 45.32; H, 5.80; N, 8.67. $C_{24}H_{36}Cl_2NiN_4O_8$ requires C, 45.17; H, 5.69; N, 8.78%).

[Cu(3)(NO$_3$)]NO$_3$. Using a similar procedure to that described for [Cu(**1**)(NO$_3$)$_2$]·0.5MeOH, blue–purple crystals were produced after recrystallization of the initial product from dichloromethane–methanol (yield 65%). Single crystals suitable for X-ray diffraction were obtained from the same solvent mixture (Found: C, 50.61; H, 6.28; N, 14.73. $C_{24}H_{36}CuN_6O_6$ requires C, 50.74; H, 6.39; N, 14.79%).

[Ni(3)](ClO$_4$)$_2$. Using a similar procedure to that described for [Ni(**1**)](ClO$_4$)$_2$, nickel(II) perchlorate hexahydrate (0.144 g, 0.395 mmol) and **3** yielded orange crystals (yield 76%) after recrystallization of the initial product from acetonitrile–water. Single crystals suitable for X-ray diffraction were obtained from the same solvent mixture (Found: C, 45.05; H, 5.58; N, 8.69. $C_{24}H_{36}Cl_2NiN_4O_8$ requires C, 45.17; H, 5.69; N, 8.78%).

[Cu(4)](NO$_3$)]NO$_3$. A similar procedure to that described for [Cu(**1**)(NO$_3$)$_2$]·0.5MeOH yielded the product as blue crystals after recrystallization from absolute ethanol (yield 53%) (Found: C, 56.45; H, 6.32; N, 12.85. $C_{31}H_{42}CuN_6O_6$ requires C, 56.56; H, 6.43; N, 12.77%).

[Ni(4)](ClO$_4$)$_2$. A similar procedure to that described for [Ni(**1**)](ClO$_4$)$_2$ yielded a product which was recrystallized from methanol to give golden yellow crystals (yield 50%) (Found: C, 50.95; H, 5.59; N, 7.55. $C_{31}H_{42}Cl_2NiN_4O_8$ requires C, 51.13; H, 5.81; N, 7.69%).

[Cu(5)(H$_2$O)](NO$_3$)$_2$·2MeOH. Copper(II) nitrate–hydrate (2/5) (0.093 g, 0.4 mmol) in absolute ethanol (5 cm^3) was added to a solution of **5** (0.22 g, 0.4 mmol) in absolute ethanol (50 cm^3). The mixture was heated for 10 min and then the green–blue solution was stirred at room temperature overnight. The volume of the solvent was reduced to 10 cm^3 and the blue–green powder that formed was filtered off. This product was recrystallised from methanol to produce blue–green single crystals (0.15 g, 45%) (Found: C, 57.71; H, 6.95; N, 10.05. $C_{40}H_{58}CuN_6O_9$ requires C, 57.85; H, 7.04; N, 10.12%).

[Cu(6)(NO$_3$)]NO$_3$. Copper(II) nitrate–hydrate (2/5) (0.35 g, 1.5 mmol) in absolute ethanol (5 cm^3) was added to a solution of **6** (cyclam) (0.3 g, 1.5 mmol) in chloroform (50 cm^3). The solution was heated for 0.5 h and the solvent was evaporated on a rotary evaporator. The residue was dissolved in dichloromethane–methanol (1 : 1) (25 cm^3) and ether vapour was allowed to diffuse into the solution over 3 days. The red–purple crystalline product that formed was recrystallized from dichloromethane–methanol (1 : 1) containing a few drops of hexane to produce needle-like crystals (0.29 g, 50%) (Found: C, 30.85; H, 6.11; N, 21.55. $C_{10}H_{24}CuN_6O_6$ requires C, 30.97; H, 6.24; N, 21.67%).

CAUTION: Perchlorate-containing complexes are potentially explosive and appropriate precautions should be in place for their preparation, handling and storage.

Results and discussion

Isolation of selected complexes

The syntheses of a range of 1 : 1 (metal : ligand) complexes by mixing hot methanol or ethanol solutions of the appropriate copper(II) or nickel(II) nitrate or perchlorate salt and ligand were generally straight forward, leading to analytically pure compounds in reasonable yields. The complexes obtained together with their conductance values in methanol are listed in Table 1. Under the conditions employed, no solid nickel(II) species of **5** were isolated, presumably reflecting weak interaction of this ion with this sterically hindered system.

Each of the copper(II) complexes incorporating nitrate anions yielded a conductance value in methanol which approximated that expected for a 1 : 1 electrolyte; thus indicating that at least one of the anionic groups is on average coordinated to (or associated with) the cation under the conditions employed. In contrast, the nickel(II) complexes with ClO_4^- anions all yielded values which fall between those expected for a 1 : 1 and a 2 : 1 electrolyte. The latter behaviour parallels that reported previously for [Ni(**6**)](ClO$_4$)$_2$ in methanol[4] and indicates that some measure of cation–anion association also occurs in the present (nickel) systems in this solvent.

UV–VIS spectral properties

The UV–VIS absorption maxima of the complexes [CuL](NO$_3$)$_2$ (L = **1**–**6**) in methanol and acetonitrile and [NiL](ClO$_4$)$_2$ (L = **1**–**4** and **6**) in acetonitrile together with maxima for the corresponding solid-reflectance spectra of both metal complex types are listed in Table 2. Both the solid state and solution spectra of the copper complexes show a broad envelope of bands in the visible region which is consistent with the presence of a copper(II)–N_4 chromophore (in which solvent or anion may occupy axial positions);[13,14] however, as commonly observed, the featureless nature of the spectra result in them being of little use diagnostically for assignment of detailed coordination geometries. It is noted that in the case of the copper complex of the tetra-benzylated derivative **5**, large shifts in the λ_{max} value occur for the copper complex between the solid state and the spectra obtained in methanol or acetonitrile, presumably reflecting differential solvent interaction with the bound metal ion.

The solid state visible spectra of the orange nickel complexes of (**1**–**4**) each shows a single band with a maximum in the range 473–488 nm, consistent with the adoption of a square planar (low spin) geometry in each case. The value obtained for the corresponding nickel complex of cyclam, [Ni(**6**)]$^{2+}$, is 459 nm. This cation[12,13] has been well documented to be square planar in both the solid state[14,15] and (in the absence of coordinating anions) also in aqueous solution;[16] in the latter solvent the absorption maximum in the visible region occurs at 450 nm (ε = 45 M^{-1} cm^{-1}).

The influence of the incremental addition of N-benzyl substituents onto the cyclam framework on the electronic structure of both the respective copper and nickel complexes is especially worthy of note. The spectra obtained for each series of metal complexes confirm the expected result that the sequential introduction of N-benzyl substituents tends to produce a change in the ligand field properties towards lower fields. For example, for the square-planar nickel complexes of **1**–**4** and **6**, the tendency

towards a shift to higher wavelengths as the number of N-benzyl substituents is increased is evident from the data presented in Table 2. Since this absorption is expected to be due primarily to the promotion of an electron from the d_{xy} to $d_{x^2-y^2}$ orbital, the variation in the absorption maximum will represent the effect of changes in the donor properties on the energy difference between these orbitals. Of course, there is the possibility that acetonitrile or dimethyl sulfoxide molecules may interact in one or both of the axial positions and thus influence the separation between the above orbitals (although the singlet ground state is certainly maintained in the solid state and essentialy maintained in solution—see below).

It is noted that a 'yellow-to-blue' interconversion was observed within the present series of $[NiL]^{2+}$ complexes dissolved in acetonitrile as evidenced by the presence of weak absorptions (typical of high-spin, distorted octahedral species) that were present alongside the main low-spin, square planar absorption that fell in the range 461–517 nm (Table 2). Jørgensen[17] first reported that the nickel(II) complex with the open-chain tetramine trien (1,4,7,10-tetraazadecane) exists in solution as an equilibrium mixture of yellow, diamagnetic square species $[Ni(trien)]^{2+}$ and blue, high-spin, octahedral species of type $[Ni(trien)(H_2O)_2]^{2+}$. This behaviour was subsequently found to be common for the nickel(II) complexes with larger open-chain tetramines, the value of the equilibrium constant for the blue-to-yellow conversion being quite dependent upon ligand structure.[18] For the complexes of the macrocyclic analogues of the linear tetramines in dilute solution and at room temperature, an equilibrium mixture of high-spin and low-spin species was found to be present only in the case of the 14-membered macrocycles cyclam and isocyclam, whereas for ligands of lower and greater ring size a complete predominance of the blue octahedral complex was found to occur.[19]

EPR studies

The X-band EPR spectra of $[Cu(cyclam)]^{2+}$ and $[Cu(\mathbf{1})]^{2+}$–$[Cu(\mathbf{5})]^{2+}$ in dimethylformamide glasses were recorded at 77 K with no major differences being observed between the members of this series, although a reasonably consistent small increase in $g_{||}$ and a matching decrease in $A_{||}$ is evident on increasing the degree of N-alkylation. The parameters obtained for the complexes are shown in Table 3.

The spectra exhibit four equally spaced lines in the parallel region, as expected from the coupling of the unpaired electron density to the copper(II) nucleus ($I = 3/2$), although no superhyperfine coupling to the nitrogen donors was observed (nor was it anticipated based on a prior study).[20] These spectra, with $g_{||} > g_{\perp}$, are typical of axially symmetric d^9 copper(II) complexes in a ground-state doublet with the unpaired electron in a $d_{x^2-y^2}$ orbital.[21] The g and $A_{||}$ values of $[Cu(\mathbf{1})]^{2+}$–$[Cu(\mathbf{5})]^{2+}$ are close to that for $[Cu(cyclam)]^{2+}$ [14,22–24] suggesting an essentially square-planar coordination geometry.[21] Moreover, the $g_{||}$ values (for $[Cu(\mathbf{1})]^{2+}$–$[Cu(\mathbf{5})]^{2+}$) are slightly higher than that for $[Cu(cyclam)]^{2+}$. The latter is consistent with a trend to higher $g_{||}$ values upon N-alkylation of tetraazamacrocycles, perhaps resulting from true square-planar coordination becoming disfavoured.[20,25]

The hyperfine coupling constant, $A_{||}$, is a more reliable indicator of distortion from square-planar towards pyramidal or tetrahedral coordination in copper(II) complexes, with lower values implying distortion. The present values in the frozen solution, ranging from 200 G for $[Cu(cyclam)]^{2+}$ to 155 G for $[Cu(\mathbf{5})]^{2+}$, are consistent with the result of X-ray diffraction experiments (see later), with tetrahedral distortion being greatest in $[Cu(\mathbf{5})]^{2+}$.

Comparison of the EPR and electronic spectroscopy parameters shows that the trend of a slight increase in $g_{||}$ and a decrease in $A_{||}$ from $[Cu(cyclam)]^{2+}$ to $[Cu(\mathbf{5})]^{2+}$ is matched by a red shift of λ_{max} (as already discussed). Both observations are consistent with the planar ligand field becoming weaker while the axial ligand field becomes stronger,[26] reflected in the energy separation of the d_{xy} and $d_{x^2-y^2}$ orbitals.

Electrochemistry

Both the copper(II) and nickel(II) series of macrocyclic complexes display waves in the cyclic voltammogram associated with M(III)/(II) and M(II)/(I) processes. In both series, $E_{1/2}$ (or E_p, for irreversible cases) values shift to more positive potentials as N-benzyl substitution is progressed. For copper, the Cu(II)/(I) couple spans ~0.9 V from $[Cu(cyclam)]^{2+}$ to tetrabenzylated $[Cu(\mathbf{5})]^{2+}$, whereas the Cu(III)/(II) couple spans ~0.3 V. Spans for the Ni(II)/(I) couple are ~0.55 V and for Ni(III)/(II) ~0.35 V, for the series from $[Ni(cyclam)]^{2+}$ to $[Ni(\mathbf{4})]^{2+}$. Results for acetonitrile at a glassy carbon working electrode are summarized in Table 4; detailed data determined at both C and Pt electrodes in both acetonitrile and acetone solvents have also been obtained. The size of the effects is consistent with the assignment of the waves as metal-centred processes, where the consequence of N-alkylation of the coordinated amine donors is sensed. Previously, two series of nickel(II) complexes of (N-methyl)cyclams have been examined,[27] the two series differing in the stereochemistry at the coordinated nitrogens. The two series, *trans*-III and *trans*-I forms, showed very little differences in the redox potentials for each N-methylated geometric pair, but an overall span of ~0.55 V from unsubstituted cyclam to tetramethylcyclam complexes was observed.

The observation of consistent anodic shifts with increasing N-alkylation for both nickel and copper is illustrated in Fig. 1. The introduction of substituents on the nitrogens has several outcomes, which can all contribute to the observed shift. The substituents raise steric bulk, and the substituents may interact sterically with any donor entering the axial sites. These substitutents will also give rise to inductive effects. It is notable that substitution on remote sites on the framework of macrobicyclic hexaamines shifts the potential of the Co(III)/(II) couple over a range of ~0.5 V, although alkyl substituents alone do not cause a marked effect in those examples.[28] N-Substitution also leads to longer M–N distances for the tertiary compared with the secondary amine donors, the weaker interaction of the tertiary amine with the metal centre stabilizing antibonding orbitals on the metal, making electron removal less favourable and electron addition more favourable. The macrocycle 'hole' size will also play a role, since the metal ions in the various oxidation states are of different sizes. Although hole size effects will show up more clearly as the overall macrocyclic framework size changes (such as when methylene groups are inserted in, or deleted from, the macrocyclic ring),[29] more subtle cavity size effects arising from N-alkylation may be present in the present series. It is anticipated that such a combination of effects contribute to the observed trends.

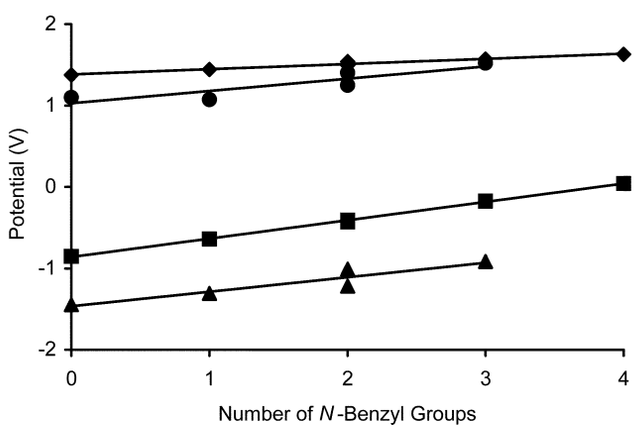

Fig. 1 Variation of redox potentials for Ni^{II-I} (▲), Cu^{II-I} (■), Ni^{II-III} (●) and Cu^{II-III} (●) couples with the number of N-benzyl groups.

The Cu(II)/(I) couples usually display quasi-reversible electrochemical behaviour, with separation of anodic (E_{pa}) and cathodic (E_{pc}) maxima in the cyclic voltammograms ranging from 75 to 250 mV and peak current ratios (I_{pa}/I_{pc}) approaching unity at 100 mV s^{-1} scan rate (Fig. 2), with typical increasing peak-to-peak separation (ΔE) as the scan rate increases. Peak current varies linearly with (scan rate)$^{1/2}$, in accordance with a diffusion controlled process; this is consistently found in the present study wherever quasi-reversibility is observed. The couples exhibit both solvent- and electrode-dependent behaviour. For example, $[Cu(\mathbf{3})]^{2+}$ at glassy carbon displays $E_{1/2} = -0.406$ V ($\Delta E = 123$ mV) in acetonitrile and -0.437 V ($\Delta E = 160$ mV) in acetone, whereas at the Pt electrode $E_{1/2}$ (ΔE) are -0.465 V (195 mV) and -0.490 V (177 mV) in acetonitrile and acetone, respectively.

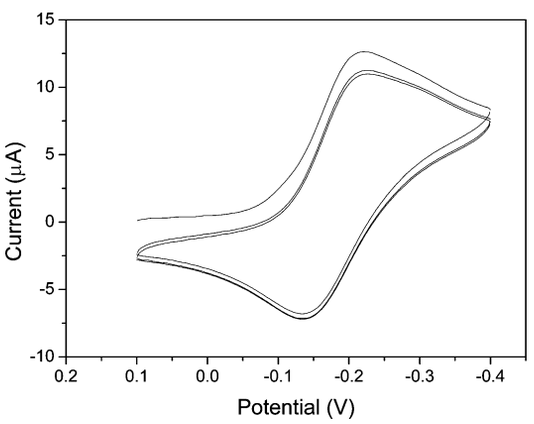

Fig. 2 Cyclic voltammogram for $[Cu(\mathbf{4})]^{2+}$. Experimental conditions: glassy carbon working electrode, 100 mV s^{-1} scan rate, 1 mmol dm^{-3} solution in acetonitrile, 0.1 mol dm^{-3} $Bu_4N(ClO_4)$ electrolyte, potentials *vs.* Ag/AgCl.

In some cases, a shift to effectively irreversible behaviour is observed, particularly at the Pt electrode. This type of electrode-dependent behaviour has also been reported in a study of a tetraalkylated-cyclam copper(II) complex.[30] The observed variation in behaviour at each electrode results from different heterogeneous electron transfer rates at the electrode surfaces, with the relatively fast electrochemical technique of cyclic voltammetry highlighting these differences. Further, the more reversible behaviour on carbon in this series possibly also reflects a greater compatibility of the complex with the surface *via* the benzene rings π-stacking with a pseudo-aromatic array of surface carbon atoms or else through the ionic complex ion-pairing to carboxylate groups arising from oxidized carbon sites on the surface.

The solvent shifts, although modest, contrast with very small solvent-dependent shifts for ferrocenium/ferrocene, suggesting solvation effects that are not simply the result of junction potential differences. Solvent effects may reflect outer-sphere solvation or even a role for solvent in the inner coordination sphere; acetonitrile is a better ligand than acetone, and can readily occupy coordination sites in expanded coordination number species. In particular, both reduction and oxidation of d^9 copper(II) remove or diminish the significant Jahn–Teller elongation of axial sites, enhancing the opportunity for solvent to bind in these sites whenever higher coordination number geometries are stabilized [although this outcome is more likely for copper(III) than copper(I)].

The electrochemical reversibility displayed implies a capacity on the timescale relevant for the complexes to adapt to geometrical changes as the oxidation state changes. For the Cu(II)/(I) couple, square planar and tetrahedral geometries may be anticipated for copper(II) and copper(I), respectively, and the ligand must be flexible enough to accommodate this transformation, as well as retain the metal ion in the macrocyclic cavity. The large N-benzyl pendants introduced may act to limit dissociation processes by their bulk, thus enhancing the reversibility of couples.

The copper(II)/(III) couple, which occurs at very positive potential, is irreversible. This is consistent with observations for copper tetraaza macrocycles generally;[29] reversibility has been reported only in very strong perchloric acid solution.[31] The irreversibility may reflect a major change in coordination geometry from the d^8 to the d^7 system, discussed above, but may equally well relate to increased lability of the copper(III) leading to a rapid following dissociation reaction in an EC mechanism, or a capacity for the powerful copper(III) oxidant to oxidize the coordinated saturated polyamine ligand. Both a parallel positive shift in potential for the M(II)/(I) and putative M(II)/(III) processes, and comparable wave-heights consistent with two one-electron processes, support the assignment of this latter wave as a metal-centred oxidation. Another wave seen for only some samples at potentials more anodic than this process as a shoulder on the edge of the solvent limit is most likely related to traces of water in the solvent.

The Ni(II)/(I) couple shifts anodically with N-substitution and consistently displays quasi-reversible behaviour (Fig. 3), albeit complicated in many cases by adsorption–desorption phenomena. However, for the Ni(II)/(III) process it is noted that two sets of waves that are quasi-reversible in character are observed, with one usually dominant in terms of peak currents. The relative size of these pairs of waves varies considerably with the nature of the ligand, solvent and electrode. However, their summed wave-heights (albeit taken from the cyclic voltammograms rather than obtained using stirred voltammetry) are essentially equivalent to that of the simple Ni(II)/(I) process (Fig. 4), which suggests that they represent components of the same overall one-electron process. The fact that the shift in each on N-alkylation follows the same trend supports this. The two processes could simply reflect adsorbed and free species, which are oxidized at different potentials according to:

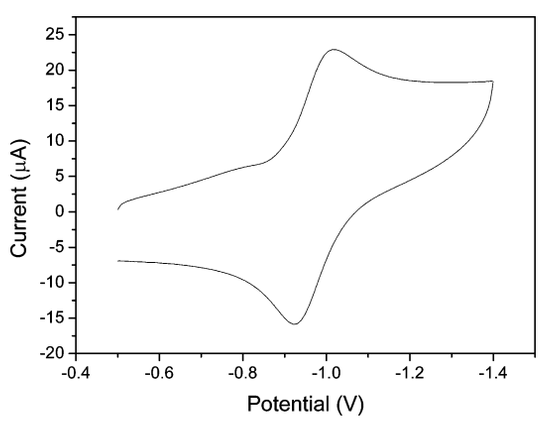

Fig. 3 Cyclic voltammogram for $[Ni(\mathbf{2})]^{2+}$ complex. Experimental conditions: glassy carbon working electrode, 500 mV s^{-1} scan rate, 1 mmol dm^{-3} solutions in acetone, 0.1 mol dm^{-3} $Bu_4N(ClO_4)$ electrolyte, potentials *vs.* Ag/AgCl.

$$\begin{array}{ccc} & LM^{n+} & \rightleftharpoons & LM^{n+}_{ads} & \\ (E_1) & e \Big\Vert - e & & e \Big\Vert - e & (E_2) \\ & LM^{(n+1)+} & \rightleftharpoons & LM^{(n+1)+}_{ads} & \end{array} \quad (1)$$

Such processes appear in some of the Ni(II)/(I) couples, where the relative size of component shoulders and peaks vary somewhat with scan speed, supporting the assignment. In the Ni(II)/(III) process the shifts are substantial (as much as ~0.6 V), and are less influenced by scan rate. More properly, they likely reflect the presence of low-spin to high-spin equilibria at the electrode surface:

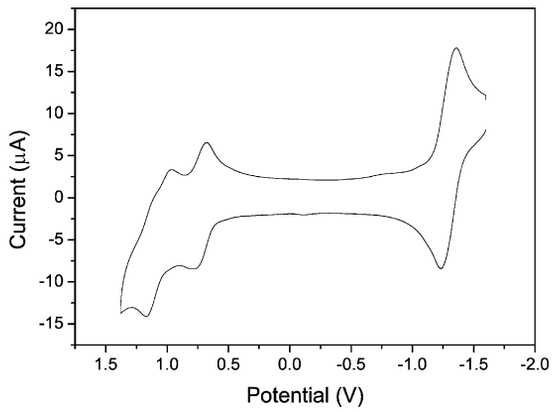

Fig. 4 Cyclic voltammogram for $[Ni(\mathbf{1})]^{2+}$. Experimental conditions: glassy carbon working electrode, 100 mV s^{-1} scan rate, 1 mmol dm^{-3} solutions in acetonitrile, 0.1 mol dm^{-3} $Bu_4N(ClO_4)$ electrolyte, potentials *vs.* Ag/AgCl.

$$\begin{array}{ccc} (L)Ni^{2+} + 2\,sol & \rightleftharpoons & (L)Ni(sol)_2^{2+} \\ (E_1)\quad e \uparrow\downarrow - e & & e \uparrow\downarrow - e \quad (E_2) \\ (L)Ni^{3+} + 2\,sol & \rightleftharpoons & (L)Ni(sol)_2^{3+} \end{array} \qquad (2)$$

The bis(solvent) complex would be expected to be oxidized at a different potential and show substantial solvent effects, as is observed. For example, with $[Ni(\mathbf{1})]^{2+}$, the positions of the pairs of waves at glassy carbon in acetonitrile (1.074, 0.734 V) differ clearly from those in acetone (1.394, 0.708 V). It is tempting to assign the more anodic wave, where shifts are greatest and the peak currents are larger, to the six-coordinate high spin form. The Ni(cyclam)]$^+$ complex in acetonitrile is known to exist as a 78 : 22 mixture of 6- : 4-coordination species,[32] supporting this proposal. Further, as mentioned already, spin equilibria have been established in solution for the compounds in this study. The complex patterns for particular Ni(II)/(I) couples may reflect similar behaviour masked by adsorption, with the absence of two processes in some cases simply relating to coincidence of reduction potentials.

Irreversible waves are observed at more negative potentials following the M(II)/(I) couples for both metals. These may be associated with formal reduction to M(0). The observation of irreversible processes near −2.0 V for tetraazamacrocyclic nickel complexes, assigned to such a process, have been reported.[33] Alternatively, as remaining amine protons become more acidic with N-substitution, abstraction of a H atom from the weaker NH bond is possible, allowing a process of the type:[34]

$$(LH)M^{n+} \xrightarrow[E_1]{-1e} (LH)M^{(n-1)+} \xrightarrow[fast]{k} H^{\cdot} + (L)M^{n+} \xrightarrow[E_2]{-1e} LM^{(n-1)+} \qquad (3)$$

However, no reverse wave near −0.45 V, seen for hydrogen-saturated acetone at the Pt electrode, is observed in the cyclic volammograms, suggesting that this process is not occurring. The Ni(II)/(I) couple for $[Ni(\mathbf{4})]^{2+}$ in acetonitrile does not shift appreciably on addition of Et_3N as base (−0.915 *vs.* −0.902 V with base), nor does the first following process (−1.49 *vs* −1.40 V with base), also not supporting a proton abstraction mechanism. Instead, for the copper complexes, a sharp oxidation peak with a Lorentzian profile, indicative of an electrode stripping process, is observed near −0.2 V; for nickel complexes, this is absent. These observations suggest irreversible processes with rapid following chemical reactions, such as would occur for reduction to M(0). Irreversible waves at very negative potential for some N-pendants including thioether functionality have been ascribed to ligand-centred processes involving this group as they are absent when this group is not present;[35] however, in the present study, no clear candidates for ligand-centred processes exist. A disproportionation reaction may also be entertained; however, given the limited information available, further speculation appears unwarranted.

It is noted that an approximately linear relationship occurs between the position of the d–d transition maximum (ν_{max}) and $E_{1/2}$ (V) for both reduction and oxidation processes for each of the copper and nickel complexes (the situation for copper is illustrated in Fig. 5). Reasons for correlations of maxima in electronic spectra with E° are not immediately obvious, although they have been reported before.[27] However, they are by no means universal; for example, an extensive series of simple $[Co(NH_3)_5X]^{n+}$ complexes show no such relationship.[36]

Electrode potential reflects differences in the energies of the $M^{n+}/M^{(n+1)+}$ ground states, whereas electronic transitions arise form different ground and excited states of M^{n+}. Nevertheless, trends in the common ground state energy may influence both properties in the same sense. To complicate the outcome, the broad absorption envelope for copper(II) is the sum of several transitions under the severely tetragonally distorted symmetry, and hence provides a fairly modest measure of ligand field strength. For nickel(II), the spin equilibria in solution discussed above complicate the situation, as shown, for example, by the distinctly different spectra for $[Ni(\mathbf{4})]^{2+}$ in solution and the solid state. Nevertheless, the existence of a relationship is in accordance with observations for other macrocyclic systems, even though exceptions occur.

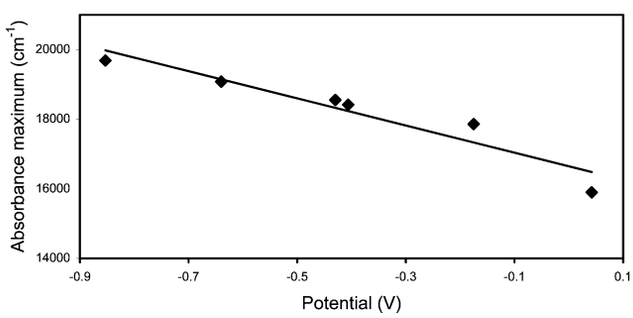

Fig. 5 The relationship between ν_{max} (solid state absorption visible spectra) *vs.* redox potentials (Cu^{II-I}) for the copper(II) complexes of **1**–**6**.

Crystal structures

ORTEP[11] depictions of $[Cu(\mathbf{1})(ONO_2)_2]\cdot 0.5MeOH$, $[Cu(\mathbf{2})(ONO_2)_2]\cdot MeOH$, $[Cu(\mathbf{3})(ONO_2)_2]$, $[Ni(\mathbf{3})](ClO_4)_2$ and $[Cu(\mathbf{5})(H_2O)](NO_3)_2\cdot 2MeOH$ are provided in Figs. 6–10 and relevent geometry details are listed in Tables 5–8. The copper(II) complex of **1**, isolated as its nitrate salt, is formulated as $[Cu(\mathbf{1})(ONO_2)_2]\cdot 0.5MeOH$. The 14-membered macrocyclic ring adopts the stable *trans*-III configuration[37] (Fig. 6), with the copper(II) situated at the centre of the macrocyclic cavity with the ligand maintained in a planar arrangement. The Cu–N(1) bond length of 2.061(4) Å (to NCH_2Ph) is slightly longer than that of Cu–N(2) 1.997(5) Å, Cu–N(3) 2.027(4) Å and Cu–N(4) 2.010(5) Å, presumably as a consequence of alkylation on the N(1) atom. The coordination sphere is completed by oxygen donors from two nitrato ligands, with a Cu(1)–O(1) bond length of 2.804(6), and a Cu(1)–O(4) bond length of 2.476(4) Å (Fig. 6, Table 5). The resulting geometry is a tetragonally distorted octahedron as is commonly found for copper(II) complexes.[38] There is a hydrogen bonding interaction between the methanol solvate molecule and the N(5) nitrate ion, and hydrogen bond interactions between the amine nitrogen atoms and the nitrate counter ions of neighbouring complex molecules (see CIF file).

The copper(II) complex of **2** is similarly formulated as $[Cu(\mathbf{2})(ONO_2)_2]\cdot MeOH$, and also has the macrocycle in a *trans*-III configuration, with the two benzyl substituents lying on the same side of the square plane of the macrocycle donors (Fig. 7,

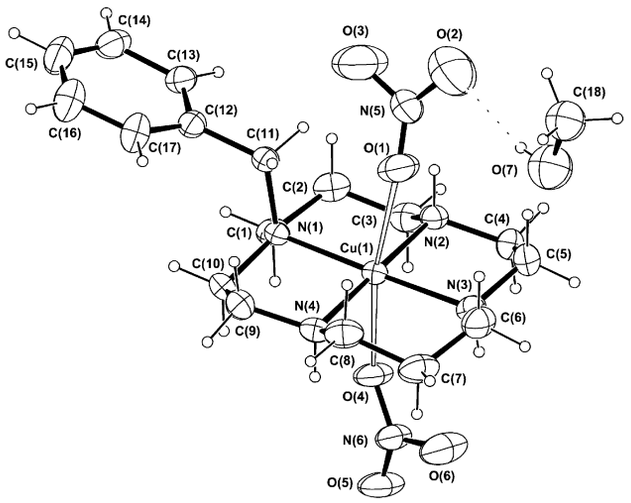

Fig. 6 ORTEP depiction of [Cu(**1**)$(ONO_2)_2$]·0.5MeOH, with 20% displacement ellipsoids.

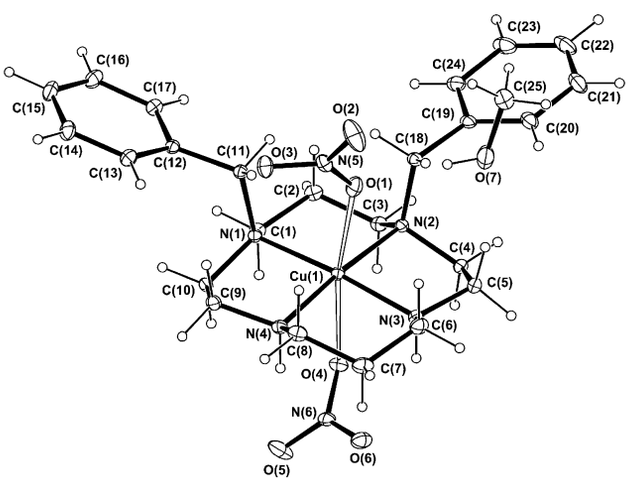

Fig. 7 ORTEP depiction of [Cu(**2**)$(ONO_2)_2$]·MeOH, with 20% displacement ellipsoids.

Table 5). As expected, the Cu–N bond lengths (to NCH_2Ph) of 2.0708(12) and 2.0719(12) Å are longer than the remaining Cu–N bond lengths (to NH) at 2.0207(13) and 2.0272(13) Å. The counter ions are weakly coordinated to the metal, with a 2.7325(16) Å Cu(1)–O(1) bond length and a Cu(1)–O(4) length of 2.5663(14) Å. There is also a hydrogen bond interaction between the coordinated nitrate atom O(1) and the methanol O(7) (see CIF file). The overall coordination geometry is a tetragonally distorted octahedron.

The nickel ion in [Ni(**3**)]$(ClO_4)_2$ has a typical square-planar coordination geometry (Fig. 8), and the cyclam ring once again adopts the *trans*-III configuration. The Ni–N bond lengths are 1.9441(16) Å (to NH) and 1.9701(15) Å (to NCH_2Ph), respectively (Table 6). Two perchlorate counter ions are located above and below the coordination plane, but are beyond bonding distances.

Like the [Ni(**3**)]$(ClO_4)_2$ complex, the Cu(**3**) analogue resides on an inversion centre (Fig. 9, Table 7); however, the copper complex is hexacoordiante with two weakly coodinated nitrate counter ions and so is formulated as [Cu(**3**)$(ONO_2)_2$]. The metal to axial ligand oxygen distance is 2.6571(8) Å. Again the 14-membered ring adopts a square-planar conformation with the amine nitrogens, respectively, adopting a *RRSS* arrangement (*trans*-III). The Cu–N bond lengths are 1.9898(13) Å (to NH) and 2.1085(13) Å (to NCH_2Ph), and the metal to nitrate oxygen bond distance is 2.6571(8) Å. There is a weak hydrogen bond between N(2) and O(2) on a neighbouring complex molecule, with a donor–acceptor separation of 2.948(2) Å (see CIF file).

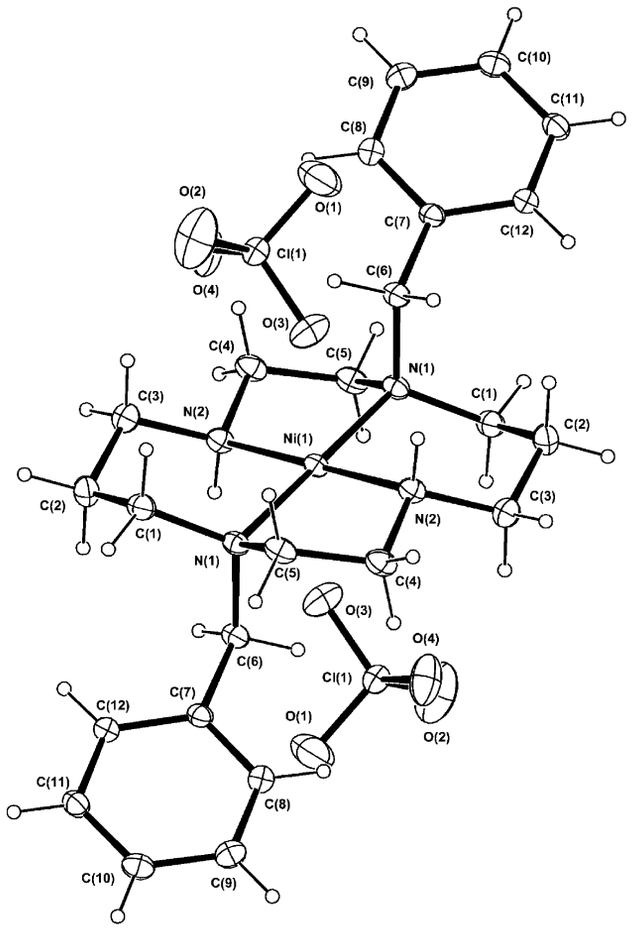

Fig. 8 ORTEP depiction of [Ni(**3**)]$(ClO_4)_2$, with 20% displacement ellipsoids. The molecule is centred on an inversion site.

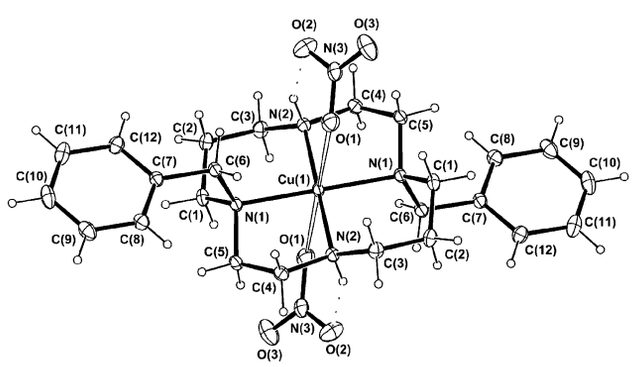

Fig. 9 ORTEP depiction of [Cu(**3**)$(ONO_2)_2$], with 20% displacement ellipsoids. The molecule is centred on an inversion site, and there are hydrogen bonding interactions between the equatorial and axial ligands.

The copper(II) complex of the tetrabenzyl derivative **5**, with additional methanol solvate molecules, is formulated as [Cu(**5**)(H_2O)]$(NO_3)_2$·2MeOH. A two-fold axis passes through the metal and coordinated water molecule (Fig. 10, Table 8). The crystal structure confirms that all four benzyl groups lie on the same side of the coordinated macrocycle in an *RSRS* configuration (*trans*-I isomer).[37] There is a pseudo-tetrahedral distortion at the copper(II) centre with the N(1)–Cu(1)–N(1) bond angle being aproximately linear at 177.08(8)° in contrast to the N(2)–Cu(1)–N(2) angle of 150.76(9)°. The Cu(1)–N(1) bond length of 2.145(2) Å is slightly longer than the 2.0841(18) Å Cu(1)–N(2) bond length. The tetrahedral distortion presumably minimises steric interactions between the benzyl side-chains and the macrocycle backbone. The five coordination sphere is completed by one oxygen donor from a water molecule. The resulting geometry approximates square pyramidal.

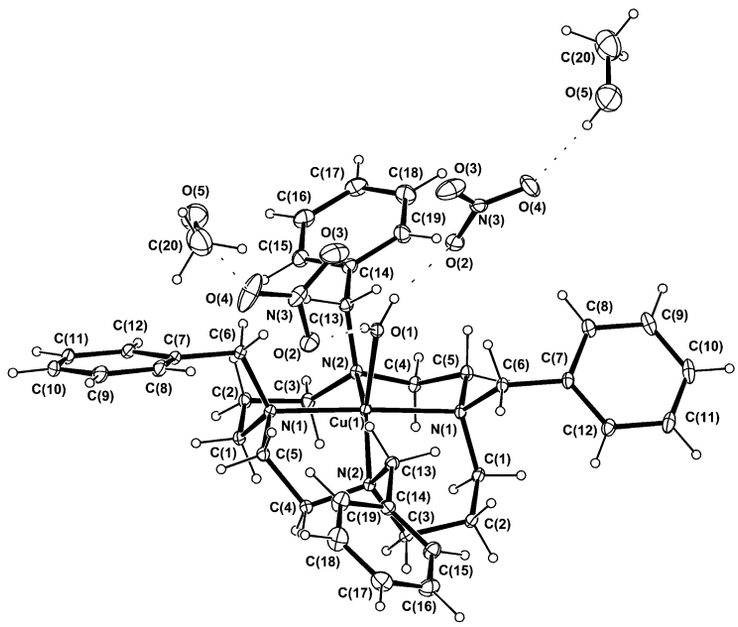

Fig. 10 ORTEP depiction of $[Cu(\mathbf{5})H_2O](NO_3)_2 \cdot 2MeOH$, with 20% displacement ellipsoids. A two fold axis passes through the axial oxygen and metals atoms.

There is a moderate hydrogen bond interaction between the nitrate counter ions and the coordinated water molecule, and between the nitrate ions and the methanol solvate molecules. The O(1) ··· O(2) donor to acceptor distance is 2.817(2), and the O(5) ··· O(4) distance is 2.779(4) Å (see CIF file).

In summary, the crystal structures of the above complexes show several features in common. First of all, the metal ion is usually situated in the centre of the macrocyclic cavity and coordinated by four nitrogen atoms from the cyclam backbone with, in many instances, oxygens from either nitrato anions or water molecules occupying axial sites. Secondly, the cyclam ring has the tendency to adopt the most stable *trans*-III configuration although the slightly less stable *trans*-I arrangement is also observed in the case of $[Cu(\mathbf{5})]^{2+}$. Finally, benzylation of nitrogen donors results in longer metal to nitrogen bond lengths than those involving secondary nitrogens in all structures.

Copper(II) solvent extraction studies

A comparative investigation of the effect of incremental N-benzylation of cyclam on the efficiency of **1**–**5** to act as extractants for copper(II) has been performed.

Clearly, the pH of the aqueous phase in a solvent extraction system may play a crucial role in influencing the efficiency of extraction of metal ions when amine-containing ligands are involved. In a previous study,[31] the copper(II) extraction efficiency of a 1:4 mixture of tetrabenzylcyclam (**5**) and palmitic acid under various pH conditions was investigated. This experiment enabled the plotting of a classical 'S-curve'; namely a curve of percent extraction against pH. For pH values less than about 5, copper(II) extraction became no longer favoured reflecting proton competition for the ligand. At pH values above about 6, competing hydrolysis occurred leading to precipitation of copper hydroxide. As a consequence of these results, pH values between 5.00 and 5.80 were chosen for the aqueous phase for the experiments undertaken in the current study.

Fig. 11 shows that, at pH 5.00 ± 0.05, the extraction efficiency increased almost linearly as the number of N-benzyl groups increased from 1 to 3, but then dropped for tetrabenzylcyclam. Related behaviour to this was observed when the pH was maintained at 5.80 ± 0.05 with the difference that for each ligand system somewhat enhanced extraction was observed at this (higher) pH—presumably reflecting lower proton competition

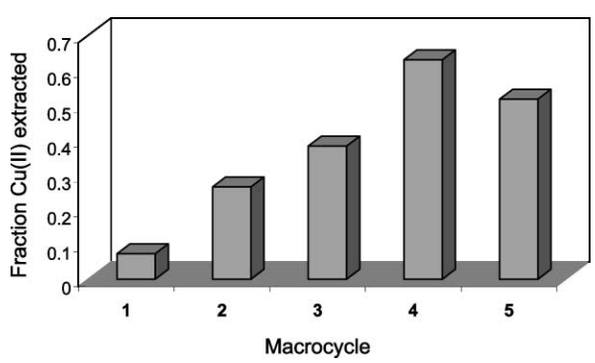

Fig. 11 The effect of increasing N-benzylation of cyclam on the efficiency of solvent extraction of copper(II). Aqueous phase: 5 cm^3, contained copper(II) nitrate with an initial concentration of 1×10^{-3} mol dm^{-3} (pH maintained at 5.00 ± 0.05). Chloroform phase: 5 cm^3, contained ligand chosen from **1**–**5** at 1×10^{-3} mol dm^{-3} and palmitic acid at 4×10^{-3} mol dm^{-3}. The extraction vial was shaken for 24 h at 25 °C.

for the ligands' amine sites. Besides pH, and as discussed previously,[39] the interplay of two further subtle factors may dominate extraction behaviour of the present type. First, the lipophilicity of ligand will play a role in influencing extraction efficiency. More lipophilic ligands (lipophilicity is expected to increase with increasing N-benzylation) may aid the extraction process by inhibiting the bleeding of the amine ligand (or its metal complex) from the organic to the aqueous phase as well as enhancing extraction through favorable solvation effects. Indeed, the appearance of a pink–violet coloration in the aqueous phase for each of the systems incorporating the less lipophilic systems **1**–**3** is attributed to bleeding of macrocycle from the organic phase under the conditions employed. Secondly, the overall thermodynamic affinity of the ligand for the metal ion of interest will also be important in influencing the efficiency of extraction behaviour. In this regard both the electronic and steric nature of the extractant may play important roles in solvent extraction. For example, when four N-substituted phenyl groups are present, as occurs in **5**, steric hindrance associated with the four benzyl substituents may be the cause of the observed somewhat reduced extraction efficiency even though the lipophilicity of this metal–ligand system might be expected to be the highest of the present series. Indeed, earlier workers found no evidence for the complexation

of either copper(II) or nickel(II) by this ligand in a number of common solvents.[40]

Acknowledgements

We thank the Australian Research Council for support.

References

1 D. Meyerstein, *Coord. Chem. Rev.*, 1999, **185–186**, 141.
2 Y. Dong and L. F. Lindoy, *Aust. J. Chem.*, 2001, **54**, 291.
3 E. K. Barefield, F. Wagner, A. W. Herlinger and A. R. Dahl, *Inorg. Synth.*, 1976, **16**, 220.
4 Bruker (1995); SMART, SAINT and XPREP. Area detector control and data integration and reduction software. Bruker Analytical X-ray Instruments Inc., Madison, WI, USA.
5 P. Coppens, L. Leiserowitz and D. Rabinovich, *Acta Crystallogr.*, 1965, **18**, 1035.
6 Molecular Structure Corporation, teXsan for Windows: Single Crystal Structure Analysis Software, MSC, 3200 Research Forest Drive, The Woodlands, TX 77381, USA, 1997–1998.
7 WinGX L. J. Farrugia, *J. Appl. Crystallogr.*, 1999, **32**, 837.
8 S. R. Hall, D. J. du Boulay and R. Olthof-Hazekamp, eds. Xtal3.6 System, University of WesternAustralia, 1999.
9 A. Altomare, M. C. Burla, M. Camalli, G. L. Cascarano, C. Giacovazzo, A. Guagliardi, A. G. C. Moliterni, G. Polidori and R. Spagna, *J. Appl. Crystallogr.*, 1999, **32**, 115.
10 G. M. Sheldrick, SHELX97. Programs for Crystal Structure Analysis, University of Göttingen, Institüt für Anorganische Chemie der Universität, Tammanstrasse 4, D-3400 Göttingen, Germany, 1998.
11 C. K. Johnson, ORTEPII. Report ORNL-5138, Oak Ridge National Laboratory, Oak Ridge, TN, 1976.
12 B. Bosnich, M. L. Tobe and G. A. Webb, *Inorg. Chem.*, 1965, **4**, 1109.
13 R. Buxtrof and T. A. Kaden, *Helv. Chim. Acta*, 1974, **57**, 1035; M. Hediger and T. A. Kaden, *Helv. Chim. Acta*, 1983, **66**, 86.
14 L. Fabbrizzi, L. Montagna, A. Poggi, T. A. Kaden and L. C. Siegfried, *J. Chem. Soc., Dalton Trans.*, 1987, 2631.
15 K. R. Adam, M. Antolovich, L. G. Brigden, A. J. Leong, L. F. Lindoy, P. J. Baillie, D. K. Uppall, M. McPartlin, B. Shah, D. Proserpio, L. Fabbrizzi and P. A. Tasker, *J. Chem. Soc., Dalton Trans.*, 1991, 2493; K. A. Adam, I. M. Atkinson and L. F. Lindoy, *Inorg. Chem.*, 1997, **36**, 480; M. A. Donnelly and M. Zimmer, *Inorg. Chem.*, 1999, **38**, 1650.
16 E. Zeigerson, G. Ginzburg, D. Meyerstein and L. J. Kirschenbaum, *J. Chem. Soc., Dalton. Trans.*, 1980, 1243.
17 C. K. Jøgensen, *Acta Chem. Scand.*, 1957, **11**, 399.
18 A. Anichini, L. Fabbrizzi, P. Paoletti and R. M. Clay, *Inorg. Chim. Acta*, 1977, **24**, L21; R. W. Hay, B. Kinsman and C. I. Smith, *Polyhedron*, 1995, **14**, 1245; L. Fabbrizzi, *Comments Inorg. Chem*, 1985, **4**, 33; A. De Blas, G. De Santis, L. Fabbrizzi, M. Licchelli and P. Pallavicini, *Pure Appl. Chem.*, 1993, **65**, 455.
19 M. Ciampolini, L. Fabbrizzi, M. Licchelli, A. Perotti, F. Pezzini and A. Poggi, *Inorg. Chem.*, 1986, **25**, 4131.
20 A. E. Geota, J. A. K. Howard, D. Maffeo, H. Puschmann, J. A. G. Williams and D. S. Yufit, *J. Chem. Soc., Dalton Trans.*, 2000, 1873.
21 H. Kurosaki, C. Bucher, E. Espinosa, J.-M. Barbe and G. Guilard, *Inorg. Chim. Acta*, 2001, **322**, 145.
22 S. V. Rosokha, Y. D. Lampeka and I. M. Maloshtan, *J. Chem. Soc., Dalton Trans.*, 1993, 631.
23 M. Lachkar, G. Guilard, A. Atmani, A. De Cian, Jean Fischer and Raymond Weiss, *Inorg. Chem.*, 1998, **37**, 1575.
24 E. Zeigerson, G. Ginzburg, D. Meyerstein and L. J. Kirschenbaum, *J. Chem. Soc., Dalton Trans.*, 1980, 1243.
25 F. E. Mabbs and D. Collison, *Electron paramagnetic resonance of d transition metal compounds*, Elsevier, Amsterdam, 1992.
26 X. H. Bu, Z. H. Zhang, D. L. An, Y. T. Chen, M. Shionoya and E. Kimura, *Inorg. Chim. Acta*, 1996, **249**, 125.
27 E. K. Barefield, G. M. Freeman and D. G. van Derveer, *Inorg. Chem.*, 1986, **25**, 552.
28 A. M. Bond, G. A. Lawrance, P. A. Lay and A. M. Sargeson, *Inorg. Chem.*, 1983, **22**, 2010.
29 E. Kimura, T. Koike, R. Machida, R. Nagai and M. Kodama, *Inorg. Chem.*, 1984, **23**, 4181.
30 R. Bilewicz and M. Pietraszkiewicz, *Polyhedron*, 1990, **9**, 2353.
31 M. Ciampolini, L. Fabbrizzi, A. Perotti, A. Poggi, B. Seghi and F. Zanobibi, *Inorg. Chem.*, 1987, **26**, 3527.
32 N. Sabatini and L. Fabbrizzi, *Inorg. Chem.*, 1979, **18**, 438.
33 F. V. Lovecchio, E. S. Gore and D. H. Busch, *J. Am. Chem. Soc.*, 1974, **96**, 3109.
34 H. A. Boucher, G. A. Lawrance, P. A. Lay, A. M. Sargeson, A. M. Bond, D. F. Sangster and J. C. Sullivan, *J. Am. Chem. Soc.*, 1983, **105**, 4652.
35 C. L. Schmid, C. Kempf, A. Taubert, M. Neuburger, M. Zehnder and T. A. Kaden, *Helv. Chim. Acta*, 1996, **79**, 1011.
36 N. J. Curtis, G. A. Lawrance and A. M. Sargeson, *Aust. J. Chem.*, 1983, **36**, 1327.
37 L. F. Lindoy, *The Chemistry of Macrocyclic Ligand complexes*, Cambridge University Press, Cambridge, 1989.
38 M. H. Meyer, P. Singh, W. E. Hatfield and D. J. Hodgson, *Acta Crystallogr., Sect. B*, 1972, **28**, 1607.
39 K. R. Adam, I. M. Atkinson, S. Farquhar, A. J. Leong, L. F. Lindoy, M. S. Mahinay, P. A. Tasker and D. Thorp, *Pure Appl. Chem.*, 1998, **70**, 2345.
40 M. R. Oberholzer, M. Neuburger, M. Zehnder and T. A. Kaden, *Helv. Chim. Acta*, 1995, **78**, 505.